Developmental effects of polystyrene nanoparticles in the chicken embryo

Wang, M.

Chapter 3. Nanoplastics cause cardiac malformations and abnormal circulation in chicken embryos

Meiru Wang[1,2], Robert E. Poelmann[1,3], Martin Rücklin[2,1], Carmen L. de Mooij[1], Gerda E.M. Lamers[1], Ernest Chin[1], Lilla J. Bakos[1], Federica Marone[4], Bert J. Wisse[5], Marco C. de Ruiter[5], Martina G. Vijver[6], Michael K. Richardson[1].*

1. Institute of Biology, Leiden University, Sylvius Laboratory, Sylviusweg 72, 2333 BE, Leiden, The Netherlands.
2. Naturalis Biodiversity Center, Darwinweg 2, 2333 CR, Leiden, The Netherlands.
3. Department of Cardiology, Leiden University Medical Center, The Netherlands.
4. Swiss Light Source, Paul Scherrer Institut, Photon Science Department, Forschungsstrasse 111, CH-5232 Villigen, Switzerland.
5. Department of Anatomy & Embryology, Leiden University Medical Center, The Netherlands.
6. Institute of Environmental Sciences, Leiden University (CML), Van Steenis Building, Einsteinweg 2, 2333 CC, Leiden, The Netherlands.

This chapter has been published as part of: Wang, M., Rücklin, M., Poelmann, R.E., de Mooij, C.L., Fokkema, M., Lamers, G.E.M., de Bakker, M.A.G., Chin, E., Bakos, L.J., Marone, F., Wisse, B.J., de Ruiter, M.C., Cheng, S., Nurhidayat, L., Vijver, M.G., Richardson, M.K. Nanoplastics causes extensive congenital malformations during embryonic development by passively targeting neural crest cells. *Environment International* **173**, 107865. https://doi.org/10.1016/j.envint.2023.107865.

Abstract

Plastic waste has become a major environmental pollutant due to the poor management of plastic waste, and its limited recyclability. Among plastic waste, there are small plastic particles, defined as microplastics (≤ 5mm diameter) and nanoplastics (≤ 1 μm diameter). It has been previously reported in the literature, and here in Chapter 2, that nanoplastics can cause malformations in the nervous system and eye. Here, we explore the range of malformations produced by nanoplastics in more depth. We exposed stage 8 chicken embryos to 25 nm plain polystyrene nanoplastics and examined these embryos at a wider range of stages than in previous studies. We find that the polystyrene nanoparticles can cause severe malformations in craniofacial and cardiovascular systems. These include major heart defects and impaired cardiac function. In addition, the severe dysplasia of the palatine, maxillary and premaxillary cartilages was observed in embryos treated with nanoplastics. Furthermore, we found abnormal expression patterns of the genes TFAP2A, TNNI and NKX2-5 in treated embryos. Combining these data with the fact that nanoplastics also cause neural tube defects (Chapter 2) we suggest that nanoplastics disrupt the cardiocraniofacial module of the developing embryo, possibly by an effect on neural crest cells. Our hypotheses will be further explored in Chapter 4.

Introduction

Microplastics and nanoplastics (MPs and NPs) are small plastic particles with relevance to human health. Both types of particle are widely present in air and drinking water (Cox et al., 2019; Koelmans et al., 2019). A further potential source of exposure, at least for humans, is that NPs are being considered as new drug delivery vehicles for use in human medicine (Boehnke et al., 2022). They are also found in house dust (Zhang et al., 2020), and are added by the manufacturer to some household and personal hygiene products (Anagnosti et al., 2021; Vighi et al., 2021). Note that some European Union member states are considering the banning of nanoplastics as components of these products (European_Commission, 2022).

Strikingly, these plastics particles have been found in the human body. For example, there were 12 different types of MPs (PP, PET etc.) detected in the tissue of human lungs from 13 volunteers (Jenner et al., 2022). Another study detected MPs in blood samples of 22 healthy human volunteers at an average concentration of 1.6 μg/mL (Leslie et al., 2022). Furthermore, NPs ranging from 50 – 500 nm have been found in human feces (Schwabl et al., 2019). These and other studies have raised public concerns about the potential health-risk that MPs and NPs may pose (Mitrano et al., 2021).

The effects of MPs and NPs have mostly been studied on aquatic organisms including crustaceans (e.g. *Daphnia*), gastropods, and fish (e.g. zebrafish) (Kögel et al., 2020). As we discussed in more detail in Chapter 1, those studies have shown that MPs and NPs can produce a range of toxic effects including growth delays, reproductive effects, developmental toxicity, behavioral abnormalities and bradycardia (Pitt et al., 2018; Wan et al., 2018).

In Chapter 2 we reported that exposure of chicken embryos to 25 nm NPs produced neural tube defects, vertebral column abnormalities and tail bud defects. These phenotypic effects were at 24 hpe – 4 dpe. In this chapter, we analyze the effects of

PS-NPs on the embryo at a wider range of stages including later ones. We chose to do this in order to look for effects on the heart and face. These are organ systems in which it is easier to detect malformations at stages later than 4 d. They are also relatively commonly affected by malformations in humans (Mai et al., 2019) and are therefore of interest if we want to understand the implications of NPs to human health, using the chick embryo model. Relatively little is known about potential effects of PS-NPs on cardiac development (Zhu et al., 2023). For example, PS-NPs cause bradycardia in zebrafish (*Danio rerio*) embryos (Feng et al., 2022; Pitt et al., 2018). Also, 20 nm PS-NPs affect the development of zebrafish embryos, resulting in pericardial edema (Sulukan et al., 2022). In addition, the exposure of chicken embryonic myocardial cells *in vitro* to PS-NPs produces oxidative stress in those cells (Zhang et al., 2022).

In Chapter 2, we showed that 25 nm plain PS-NPs are teratogenic to developing chicken embryos. We found malformations in the neural tube, eye, vertebral column and tail bud of early stage chicken embryos. In this chapter, we have investigated the longer-term effects of PS-NPs on chick embryo development. In particular, we were interested to see if there were effects on the heart and limbs, for example, by examining the PS-NPs-treated chick embryos at later stages of development. To study heart development in more depth, we used the markers cardiac troponin I (TNNI) which is expressed in the cytoplasm of cardiac muscle, or myocardium (Abd-Elgaliel and Tung, 2012); and the homeobox gene NKX2-5 which is expressed in the nuclei of precardiac as well as myocardial cells (McCulley and Black, 2012). Furthermore, we also examined the expression of TFAP2A (transcription factor AP-2 alpha; AP-2α) which is essential for cardiac morphogenesis (in the mouse model) (Bamforth et al., 2001; Brewer et al., 2002).

Materials and Methods

In ovo embryo toxicity experiments

We have described in Chapter 2 the detailed protocol for introducing PS-NPs into the chicken egg. After the PS-NPs were introduced, the eggs were then sealed with Scotch® prescription label tape 800 (clear) and returned to the incubator for an additional 3, 4, or 8 d (post exposure). Embryos were harvested from the egg into cold phosphate buffered saline (PBS) for further analysis.

Heart-rate recordings and analysis

The embryos were exposed *in ovo* as described in the previous section. After 2–3 d of further exposure, the embryos were placed, still in the egg, in a cradle of crumpled aluminum foil in a digitally controlled heat block (38 °C). Video recordings were made of the live embryo *in ovo* using a Nikon SMZ800 stereo microscope fitted with a Dino-Eye eyepiece camera (Dino-Lite Europe, Almere).

To determine the heart rate of chicken embryos, 27 videos were analyzed using ImageJ (v. 1.53q Java 1.8.0_322, National Institutes of Health, USA) with a custom script written by Joost Willemse (institute of Biology, University of Leiden). Videos were assembled into an image stack. Then, an area of the heart was selected using the rectangle tool in ImageJ so that the heartbeat would be registered by a change in color. The mean grey value of the selected area was calculated for each frame of the video.

Alcian blue wholemounts

This protocol is as previously described by us (de Bakker et al., 2013). Embryos were fixed with 5% trichloroacetic acid at 4 °C degree overnight. They were then transferred into refresh 70% ethanol for 2 h × 2 followed by acid alcohol (20% glacial acetic acid in 70% ethanol for 2 h). Embryos were then stained in 0.03% (W/V) Alcian blue in acid alcohol overnight. Then they were rinsed with acid alcohol for 2 h

followed by dehydration through a graded ethanol series from 70% to 100%. Finally, embryos were cleared and stored in methyl salicylate.

Histology

Paraffin histology with haematoxylin and eosin staining

We performed routine paraffin histology with haematoxylin and eosin staining according to standard protocols (Bancroft and Gamble, 2008). Embryos were fixed in 4% buffered depolymerized paraformaldehyde (pFA) for 24 h at 4 °C. They were then were washed 3x with cold PBS and dehydrated in 70% ethanol overnight. Subsequently, the embryos were dehydrated through a graded ethanol series (80%, 90%, 100%), 1 h each. Embryos were cleared with Neo-Clear® (Merck, Darmstadt), 3x 1h, and embedded in paraffin (Paraclean, KP Klinipath/VWR International, Amsterdam) at 60 °C (1x overnight, 1x 1 h). Serial sections were cut at 7 µm. Because embryos examined at 24 h post-exposure were delicate and difficult to handle, we used a modified protocol (McClelland et al., 2016). After fixing the embryos, they were embedded in a mixture of 2% agarose (Sigma-Aldrich, Zwijndrecht, A-6013) and 2.5% low melting-point agarose (super fine resolution agarose, Electron Microscopy Sciences, Hatfield, PA) at 42 °C. When the mixture had solidified at room temperature (c. 20 min), the agarose blocks containing the embedded embryos were transferred to 70% ethanol for 2 d. They were then dehydrated in graded ethanols, embedded in paraffin and sectioned. The only modification made to the embedding step was that the tissue blocks were in molten paraffin for no more than 3x 1 h.

Paraffin histology with haematoxylin, eosin and Alcian blue triple-staining

This technique helped us to visualize cartilage and the also cardiac jelly in the endocardial cushions of the heart. The protocol was done using standard haematoxylin and eosin staining with some modifications. Briefly, the 7 µm section paraffin sections were mounted on slides. They were then dewaxed in refresh xylene 3 × 5 min. Then sections were then rehydrated through 100%, 90%, 80%, 70%

ethanol. Sections were stained with Alcian blue for 10 min, followed by rinsing in tap water for 10 min. The rest of the processes is the same as with standard as haematoxylin and eosin staining (Chapter 2). The sections were subsequently stained with haematoxylin and eosin. Finally, the stained sections were cleared with xylene and mounted by Eukitt® Mounting Medium (Agar Scientific, UK).

Synchrotron X-ray tomographic microscopy

For synchrotron X-ray tomographic microscopy (synchrotron scanning) embryos were harvested and fixed in a mixture of 2.5% paraformaldehyde (pFA), 1.5% glutaraldehyde in 0.1 M sodium cacodylate buffer (pH 7.4) at 4° C for 24 h as previously described (Cotti et al., 2020). They were then dehydrated in a graded ethanol series (25%, 50%, 70%). The hearts were dissected and stored in 0.2 mL PCR tubes in 70% ethanol at 4°C. Synchrotron scanning was performed at the TOMCAT (tomographic microscopy and coherent radiology experiments) beamline (Stampanoni et al., 2006), Swiss Light Source, Paul Scherrer Institute, Villigen, Switzerland. The samples were fixed to scanning electron microscopy stubs with beeswax. The X-ray beam energy was 17 keV. For the overview scans, the microscope (Optique Peter, Lentilly, France) magnification was set to 4x. To be able to laterally cover the entire sample, the rotation axis was displaced to the side of the field of view and 2,501 projections, equiangularly distributed over 360° , were acquired with a sCMOS camera (PCO.edge, Kehlheim, Germany). To fully cover the sample in the vertical direction, a sequence of 3–4 scans was necessary. The exposure time per projection was 50 ms and the X-rays were converted into visible light with a 100 µm thick Ce doped LuAG (lutetium aluminium garnet) scintillator screen (Crytur, Turnov, Czech Republic). The effective pixel size was 1.625 µm and the sample-detector distance 20 cm. For the higher resolution scans of specific details, a 10x objective with a thinner (20 µm) scintillator of the same material was used, resulting in a pixel size of 0.65 µm. The rotation axis was positioned in the middle of the field of view, and 1,501 projections, equiangularly distributed over 180 °, were acquired with an exposure time per view of 200 ms. Prior to tomographic reconstruction (Marone et

al., 2017), all projections were dark- and flat-field corrected as well as phase-retrieved (Paganin et al., 2002). The images were analyzed and manipulated using Avizo software (Version: 8.01; Thermo, Fisher Scientific).

RNA extraction and cDNA synthesis

The RNA was isolated from stage 13-16 chick embryos by TRIzol™ Reagent (Thermo Fisher Scientific, USA) in house followed by purification with RNeasy Mini Kit (50; Qiagen, Venlo, Netherlands). The concentration of purified RNA was measured by Nanodrop. To generate first strand cDNA, we performed two-step reverse transcription polymerase chain reaction (RT-PCR) using SuperScript III (Invitrogen™, USA). The cDNA was diluted 10 × with DNA- and RNA-free water and stored at -20 °C (Sigma).

Probe synthesis

This protocol is as previously described by us (de Bakker et al., 2013). In brief, we isolated total RNA from an embryo using TRIzol (Invitrogen) and carried out reverse transcription using SuperScript III (Invitrogen). PCR was performed on these templates using specific primers (Supplementary Data Table 1), and the PCR products were cloned in the TOPOTA-PCRII vector (Invitrogen™). The inserted amplicons were checked by a PCR with M13-pUC primers located on the TOPOTA-PCRII plasmid and checked on an agarose gel. When they were of the right size, they were sent for Sanger sequencing (BaseClear B.V., Leiden). After checking the sequence by BLAST searching, the positive results were used as templates for making the digoxigenin labelled antisense RNA probes. See Supplementary Data Table S4 for accession numbers.

Wholemount *in situ* hybridization

In this study, all gene names are according to Ensembl for *Homo sapiens* (https://www.ensembl.org/). This wholemount protocol is as previously described by us (de Bakker et al., 2013). In brief, embryos were fixed in 2% buffered

depolymerized pPFA for 24 h at 4 °C. They were then washed 3 × with cold PBS and dehydrated through a graded methanol series (25%, 50%, 75% and 100%) and stored at -20 °C . Embryos were rehydrated through a graded methanol series, lightly digested with proteinase K (10 mg/mL in PBS) for 5 min and postfixed in 4% buffered pFA in PBS after several washes in PBST (PBS pH 7.2 with 0.1% Tween-20). This was followed by a prehybridization step at 60 °C for at least 3 h or until the embryo had sunk. The hybridization mixture consisted of: 50% formamide, 2% Boehringer blocking powder, 5 × SSC (from 20× standard sodium citrate buffer, 3M sodium chloride, 0.3M sodium citrate, pH 7), 1mg/mL total RNA, 50 µg/mL heparin, 0.1% Triton X-100, 0.1% CHAPS (3-[(3-cholamidopropyl) dimethylammonio]-1-propanesulfonate) and 5mM ethylenediaminetetraacetic acid (EDTA). After the prehybridization mix was removed, we added 400 ng/mL specific probe to fresh hybridization mixture preheated to 60 °C. The embryos were incubated in this mix at 60 °C overnight with slow shaking. The next day, the specific probe mixture was removed, collected and stored at -20 °C for re-use. Several stringent washes were done at 60 ° C to remove non-specifically bound probe [2× SSC, 0.1% CHAPS, 50% formamide]; [2× SSC 0.1% CHAPS]; [0.2× SSC, 0.1% CHAPS]. After washing several times at room temperature with TBST (0.1M tris [tris (hydroxymethyl)aminomethane] buffered saline, pH 7.5, 0.1% Tween-20) the embryos were preincubated with heat-inactivated 10% sheep serum in TBST for 90 min at room temperature followed by overnight incubation with sheep anti-digoxigenin conjugated to alkaline phosphatase (Roche; 1:5,000 dilution in 10% sheep serum in TBST at 4 °C overnight).

The next day, the non-specifically bound antibodies were washed away by several washes with TBST of which the last one was overnight at 4 °C. The embryos were brought to a higher pH by washing 3x 10 min in NTT buffer (0.1M sodium chloride, 0.1M Tris/HCl, 0.1% Tween-20, pH 9.5). The enzyme reaction of alkaline phosphate with BM purple (Roche) as substrate results in a blue precipitate. The development of the stain was checked regularly and stopped by washing several times in TBST, removing the substrate and chromogens, and lowering the pH.

Sectioning of wholemount *in situ* hybridized embryos

The protocol had been described in Ref. (Xu and Wilkinson, 1998). In order to get better results, we modified some steps. Chick embryos treated as described above under the subheading 'Wholemount *in situ* hybridization' were fixed in 2% PFA in PBS overnight, and the next day washed 3x 10 min with TBST on shakers at low speed. Then, the embryos were dehydrated through a graded methanol series (25%, 50%, 75%, 100%), and washed 3x in isopropanol (purity ≥ 99.5%, Sigma-Aldrich Cat.190764-1L) before being put into xylene as the intermediate reagent.

Immunochemistry

Chicken embryos (3 dpe) were fixed and dehydrated as described above under 'Wholemount *in situ* hybridization'. They were then processed for paraffin histology using standard protocols (Bancroft and Gamble, 2008). Immunochemistry was performed on 7 µm sections mounted on silane-coated slides (VWR International B.V, Amsterdam). Slides were rehydrated through 2x xylene, a graded ethanol series (100%, 90%, 80%, 70%), and demi water. Slides were then transferred to a container with 0.01 M sodium citrate buffer and heated in a microwave oven to 97 °C. When the slides cooled to room temperature, they were rinsed in PBST. We purchased all first antibodies from the same company (Santa Cruz Biotechnology in California, USA). The first antibody mix including Troponin I (H-170; cat. number ab087; dilution 1:500), anti-AP-2α (3B5; cat. number sc-12726, dilution 1:200), and Nkx.2.5 (N-19; cat number ab0266; 1:2000) was diluted in 1% bovine serum albumin (BSA) in PBST. The first antibody mix was added to the slides simultaneously. Then the slides were returned to a humidified chamber inside an incubator and incubated overnight.

The slides were rinsed in PBST. The second antibody mix contained: Alexa Fluor® 488 (Donkey anti-rabbit; cat. number AB0941, dilution: 1:200), Alexa Fluor® Plus 555 (Donkey anti-Mouse; cat. number AB1661, dilution: 1:200) and Alexa Fluor® Plus 647 (Donkey anti-Goat; cat. number ab1424) was added to the slides. All second antibodies were purchased from Thermo, Fisher Scientific USA. After rinsing with

PBST, the slides were then stained with DAPI (1:1000) for 5 min. Finally, they were washed 3x with PBST and mounted with ProLong Gold antifade reagent (Invitrogen, USA). The slides were scanned using a Zeiss Axio Scan.Z1 microscope slide scanner. High magnification views were made using a Nikon AX confocal microscope.

Results

Nanoplastics cause malformations in multiple organ systems

In treated embryos analyzed at 8 dpe, 2/6 had craniofacial dysplasia, 2/6 had cleft primary palate, 1/6 had both, and 1/6 had no craniofacial malformations (Fig. 3-1 and Table S3). The embryos with craniofacial dysplasia lacked the palatine, maxillary and premaxillary cartilages. In three cases, Meckel's cartilage was present, but not fused in the midline. There were no craniofacial malformations in the controls (*n* = 6). Embryos with neural tube defects showed concomitant vertebral defects (spina bifida; Fig. 3-1).

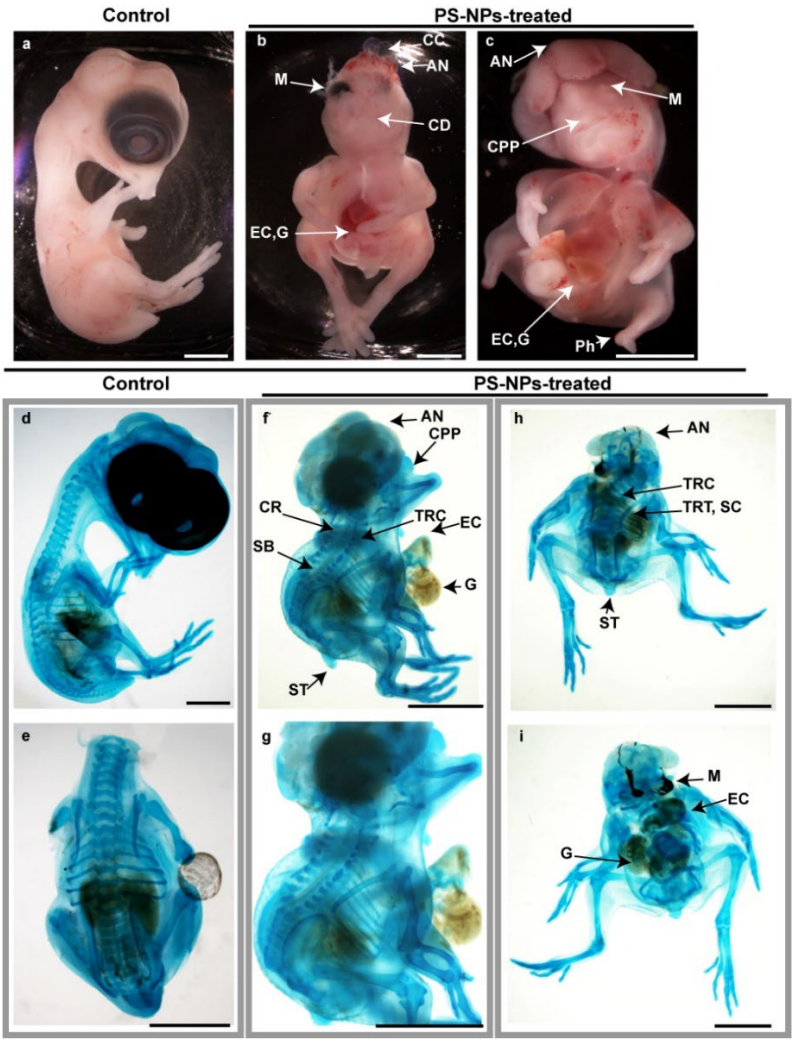

Fig. 3-1. **Gross appearance of chicken embryos examined at 8 day post exposure**. Gross appearance of embryos in control (**a**, **d**, **e**) and PS-NPs-treated group (**b**, **c**, **f**-**i**) all chicken embryos at stage 35. *Key*: AN, Anencephaly; CD, Craniofacial Dysplasia; CPP, Cleft Primary Palate; CR, Craniorachischisis; EC, Ectopia Cordis; M, Microphthalmia; Ph, Phocomelia; Sc, Scoliosis, TRC, Truncated Cervical Vertebrae; TRT, Truncated Thoracic vertebrae; ST, Short Tail, SB, Spina bifida. Scale bars are all 5 mm.

Nanoplastics cause abnormal circulatory function

When we examined living embryos *in ovo*, we found that PS-NP treated embryos showed a significant decrease in heart rate (bradycardia) at 3 dpe (Fig. 3-2). There was no significant effect on heart rate in embryos at 2 dpe.

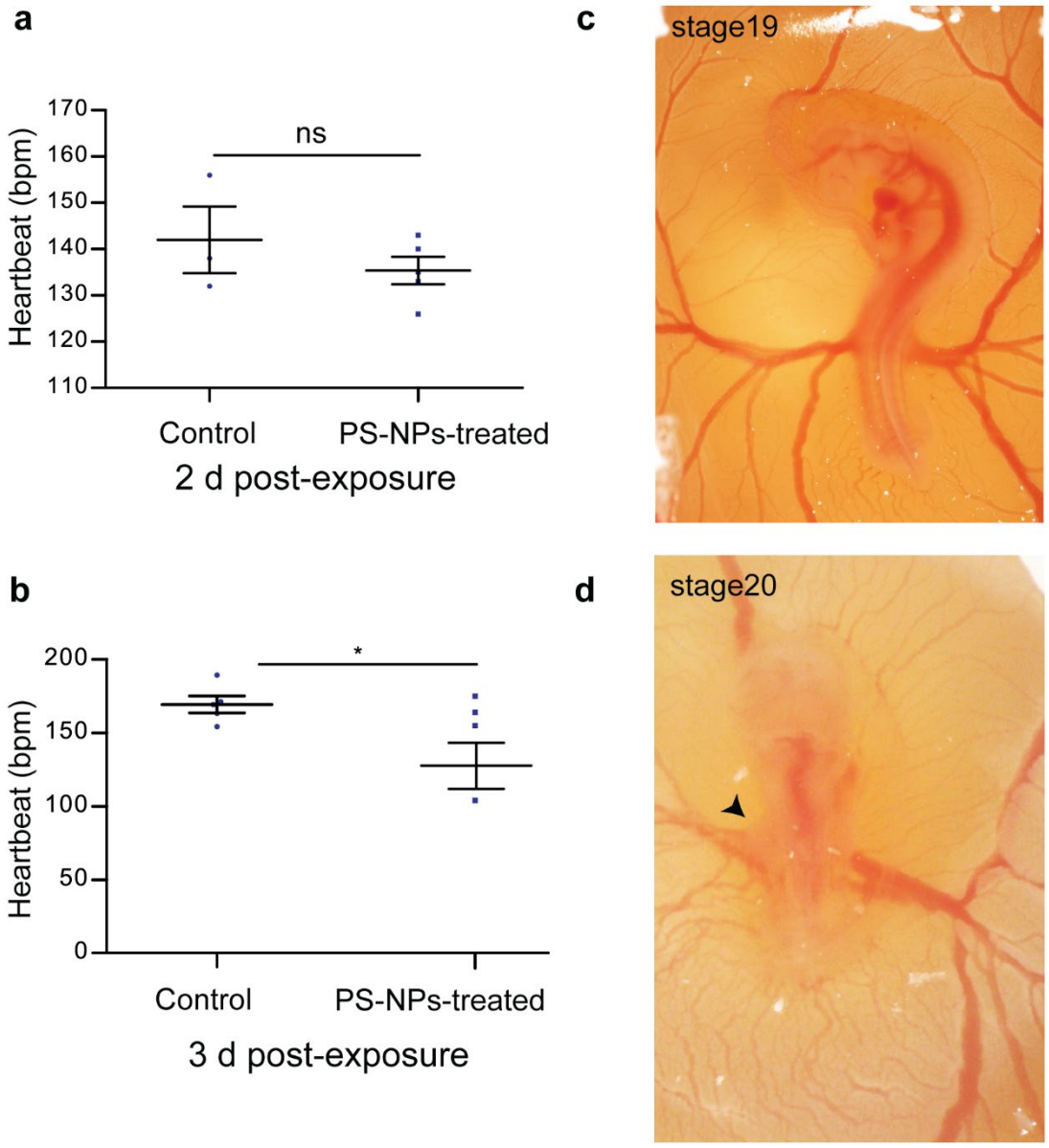

Fig. 3-2. **Heart rate and blood vessels abnormalities**. Heart rate (bpm) of 2 dpe (**a**) and 3 dpe (**b**) chick embryos, based on videos in ovo. **a**, 2 dpe chick embryos (*n* = 3 for control and *n* = 5 for PS-NP-treated). **b**, 3 dpe chick embryos (*n* = 5 for control and *n* = 4 for PS-NP-treated). **a** and **b**, data are mean ± s.e.m. Welch's t-test, P = 0.1148 for 2 dpe and P = 0.0458 for 3 dpe. **b** and **d**, chicken embryos at 2 dpe of control (**c**) and PS-NPs-treated (**d**). **c**, stage 19. **d**, stage 20, the symmetric vitelline (arrowhead) of the embryo, the left branches (arrowhead) are smaller.

Heart malformations in nanoplastic-treated embryos

One abnormality noted in PS-NPs treated embryos was an abnormal widening of vitelline blood vessels (Fig. 3-2). In some of the PS-NP treated embryos, the two dorsal aortae fuse ectopically. PS-NP treated embryos also show signs of cardiac defects when examined alive, *in ovo*, at 2 and 3 dpe. There was an abnormal abundance of cardiac jelly which continued into the apex of the heart in treated

embryos. Furthermore, the cardiac jelly appeared to be less cellularized (Fig. 3-3), most likely because of a diminished endothelial-mesenchymal transition in the endocardial lining. The myocardium also showed signs of being abnormally thin in the treated embryos (Fig. 3-3). We could not quantify any of these features in the live animals because of the rapid heartbeat.

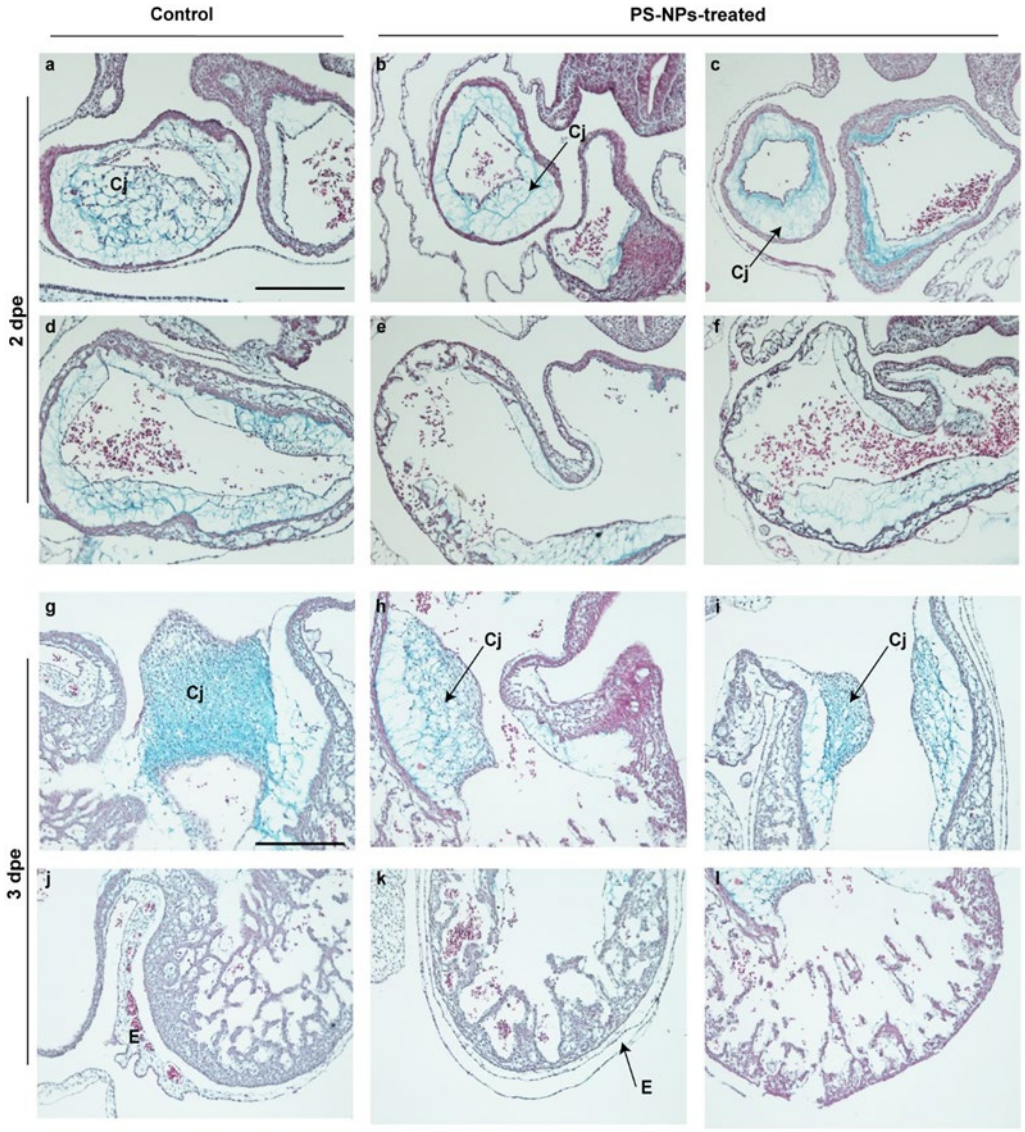

Fig. 3-3. **Heart malformation at 2 dpe and 3 dpe**. **a**-**l**, Transverse section stained with H&E and Alcian blue of **a**-**f** 2 dpe and **g**-**l** 3 dpe chick embryos. **a** and **d** control embryo, dark-stained nuclei in the cardiac jelly. **b** and **c**, PS-NPs-treated embryos, the lack of dark nuclei in the cardiac jelly is obvious. **e** and **f**, PS-NPs-treated embryos, the myocardium is thinner compared to the control embryo. **g** and **j**, heart of control embryo, note the amount of dark-stained nuclei in the cushions otherwise filled with proteoglycan-rich matrix (blue). **h** and **i**, heart of NPs treated embryo, lacking nuclei in the cushions particularly near the endocardial lining. The myocardial face of the cushion is relatively poor in matrix reflecting a defect in synthesis of the myocardium. **n**, heart of control embryo, the epicardium on the outside of the heart contains epicardium-derived cells (EPDCs) and small blood vessels. **k** and **l**, PS-

NPs-treated hearts, note the absent (**l**) or thin epicardium on the outside of the heart lacking EPDCs and blood vessels, and a thin less-trabeculated myocardium (**k**). *Key*: dpe, days post-exposure; PS-NPs Treated, polystyrene nanoparticles (5 mg/mL) treated; Cj, cardiac jelly; E, Epicardium; Scale bars are 250 µm. error bars, mean ± s.e.m.; significance of difference between control and experimental groups indicated by asterisks, *P <0.05.

Synchrotron scanning and histological sections at 8 dpe show malformations of the heart and great arteries (Fig. 3-4, Fig. 3-5, Table S3) in treated embryos. Of seven PS-NP treated embryos, three had a ventricular septal defect (Fig. 3-4h-j and n, Table S3), two had persistent or extra pharyngeal arch arteries (Fig. 3-5e-h, Table S3), one had persistent truncus arteriosus (Fig. 3-5j, Table S3) and two had aortopulmonary septal defects (Fig. 3-4o, Table S3).

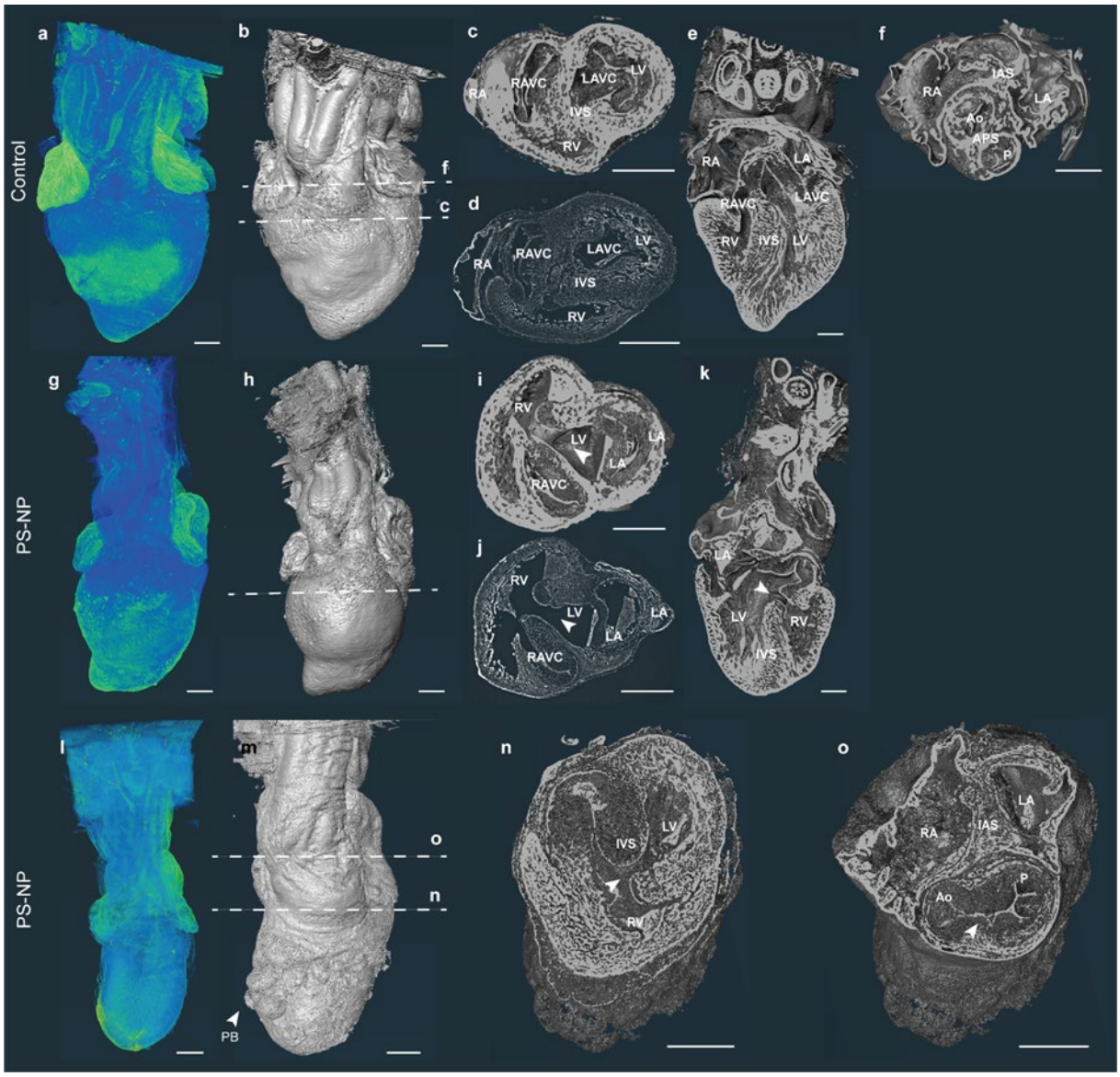

Fig. 3-4: **Synchrotron tomographic scans of hearts at 8 dpe**. **a**-**f**, control embryo, stage 35. *n* = 2. **g**-**o**, PS-NPs-treated embryos, both are stage 35. *n* = 2. (**b**, **c**, **d**, **f**), virtual sections of control embryo. (**i**, **j**, **n**, **o**), virtual transverse sections of PS-NPs-treated embryos. (**i**, **j**, **n**), virtual section at the top of the interventricular septum, with VSD (white arrow). **k**, **o**, virtual sections of the base of the outflow tract, showing APSD (white arrowhead). *Note*, treated heart in **l**-**o** both have aorticopulmonary septal defect (white arrowhead) and ventricular septal defect (white arrowhead). Key: Ao, Aorta; APS, Aorticopulmonary Septum; APSD, Aorticopulmonary Septal Defect; PB, Pericardial Blebbing; IAS, Interatrial Septum; IVS, Interventricular Septum; P, Pulmonary; LA, Left Atrium; LV, Left Ventricle; LAVC, Left Atrioventricular Canal; RA, Right Atrium; RV, Right Ventricle; RAVC, Right Atrioventricular Canal; VSD, Ventricle Septal Defect. Scale bars, 200 μm in **a**-**b**, **g**-**h**, **l**-**m** and 500 μm in **c**-**f**, **i**-**k** and **n**-**o**.

Effects of PS-NPs on expression of AP-2α and NKX2-5 genes

The analysis of 2 dpe chick embryos

We compared the wholemount *in situ* hybridization expression pattern of TFAP2A between control and NP-PS-treated embryos. In the control embryo (Fig. 3-6a), strong expression is seen in the telencephalon, in and around the eyes and in the pharyngeal arches, while less staining is observed in the area of the olfactory pit. All of the pharyngeal arches (maxilla, mandibular, hyoid, and arches 3, 4 and 6) show expression. TFAP2A is also expressed in the isthmus between the mesencephalon and the metencephalon. In contrast, we found a different expression pattern in the NP-PS-treated chick embryos (Fig. 3-6b-d). We noticed expression of TFAP2A was reduced in pharyngeal arches 3, 4 and/or 6 (Fig. 3-6b-d). Furthermore, the expression was observed to persist in the dorsal middle line or on the edges of neural folds (Fig. 3-6b and c), instead of disappearing as it did in the controls (Fig. 3-6a).

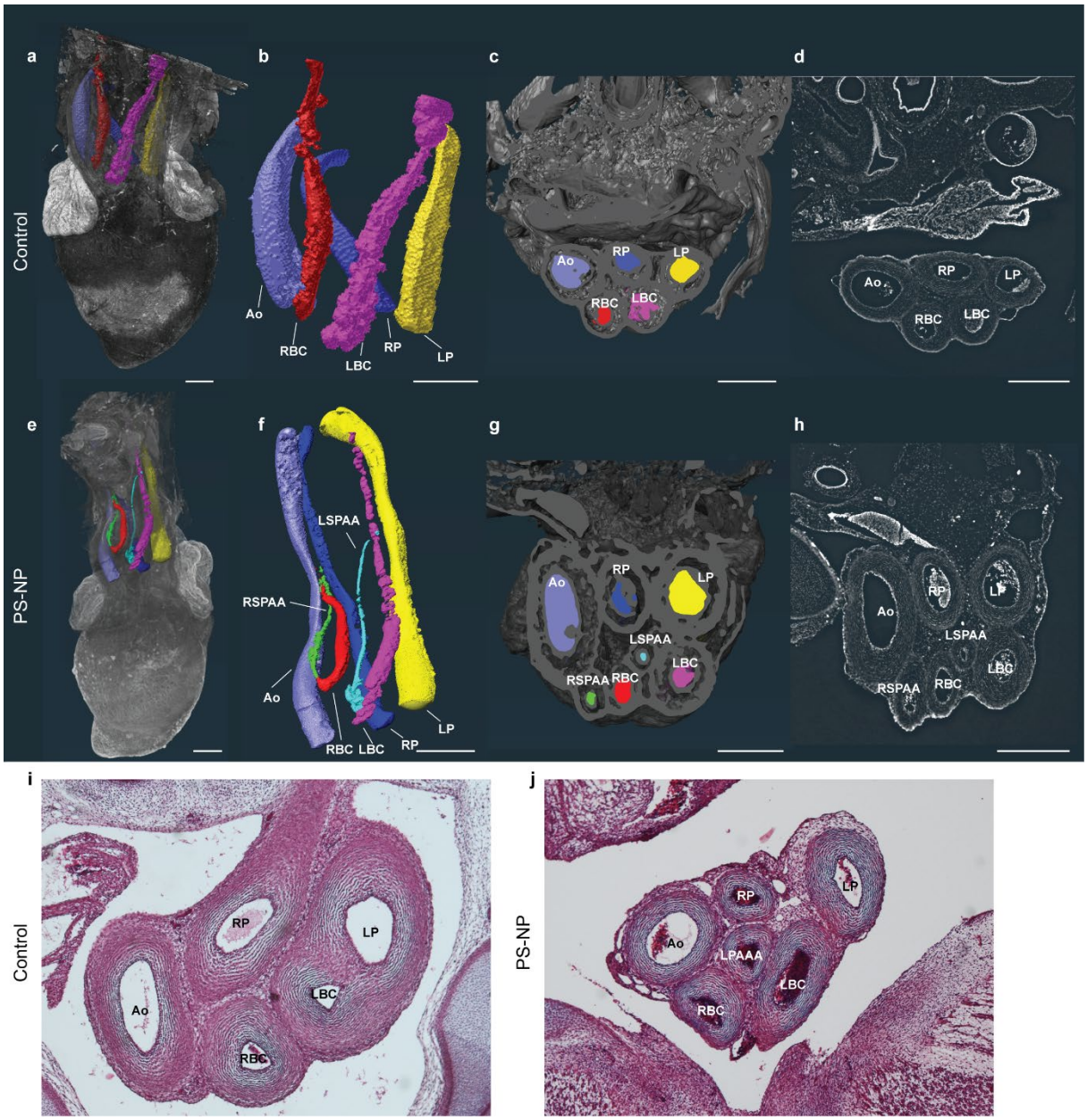

Fig. 3-5. **Synchrotron tomographic scans and transverse section of hearts at 8 dpe**. **a**-**h**, synchrotron tomographic scans of hearts and great vessels at 8 dpe. **a**-**d**, control embryo, stage 35. **e**-**h**, PS-NP treated, stage 35. **a** and **e**, volume rendering of heart and vessels. **b** and **f**, three-dimensional (3-D) model of great vessels produced by manual tracing. **c** and **g**, three-dimensional (3-D) view of virtual transverse sections. **d** and **h**, two-dimensional (2-D) view of virtual transverse sections. Transverse paraffin sections stained with H&E and Alcian blue of 8 dpe control (**i**) and PS-NPs-treated (**j**) chicken embryos. Key: Ao, Aorta; LAA, Persistent Left (4th) Aortic Arch Artery; LBC, Left Brachiocephalic Artery; LP, Left Pulmonary Artery; LSPAA, Left Supernumerary Pharyngeal Arch Arteries; RBC, Right Brachiocephalic Artery; RP, Right Pulmonary Artery; RSPAA, Right Supernumerary Pharyngeal Arch Artery.

In the case of the protein (AP-2α) of the gene TFAP2Athe expression pattern also differed between control and NP-PS-treated chick embryos. The location of AP-2α protein in pharyngeal arches is asymmetric. Particularly, in the Fig. 3-6g we see AP-2α

expression in the endoderm on one side of the arches, but barely in the other side. However, the AP-2α expression was found in ectoderm on both sides Fig. 3-6g. Interestingly, we found a cluster of cells expressing AP-2α appearing to be 'trapped' on the top of neural folds (Fig. 3-6g and h), as though they had not migrated out normally.

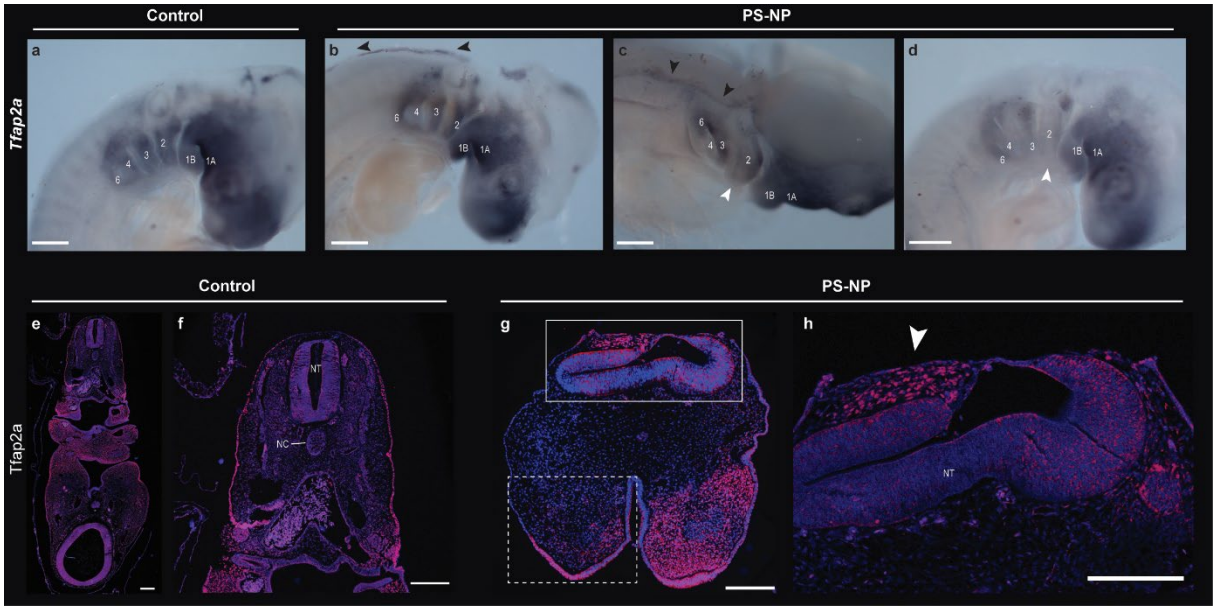

Fig. 3-6. **PS-NPs disrupt cardiac neural crest cell development in chicken embryos**. **a**-**d**, wholemount in situ hybridization for TFAP2A. **a**, control embryo, stage 19. *n* = 2. **b**-**d**, PS-NPs treated embryos, stage 18. **e**-**h**, immunochemistry showing TFAP2A (AP-2α protein; red channel) and DAPI (blue channel), transverse sections. *n* = 2 for control and *n* = 5 for PS-NPs-treated group. **e** and **f**, control chicken embryo, stage 19. **g** and **h**, PS-NPs treated embryo, stage 17. Key: black arrowhead in **b** and **c**, crest cells that apparently failed to migrate from the neural tube; white arrow in **c** and **d**, weaker expression of TFAP2A compared to control embryos. White dashed box in **g**, lack of AP-2α expression in one side of the arches. White arrowhead in **h**, some crest cells never leave the neural tube. Key: 1A, maxilla; 1B, mandible; 2, hyoid arch; 3, pharyngeal arch III; 4, pharyngeal arch IV; 6, pharyngeal arch VI; NT, neural tube; NC, notochord. Scale bars in **a**-**d**, 300 µm; in **s**-**v,** 200 µm. Blue, DAPI nuclear staining. Red, TFAP2A protein staining.

Both cardiac TNNI and NKX2-5 protein expression was compared between control and PS-NPs-treated embryos at 2 dpe (Fig. 3-7). The heart tube of the PS-NPs-treated embryos was less differentiated than that of control embryos, making it harder to distinguish the atrium from the ventricle. In the myocardium of the atrium and ventricle, similar expression patterns of cardiac TNNI and NKX2-5 are observed (Fig. 3-7a-d). DAPI staining showed that there are almost no nuclei present in the endocardial cushions of the heart (Fig. 3-7c and d).

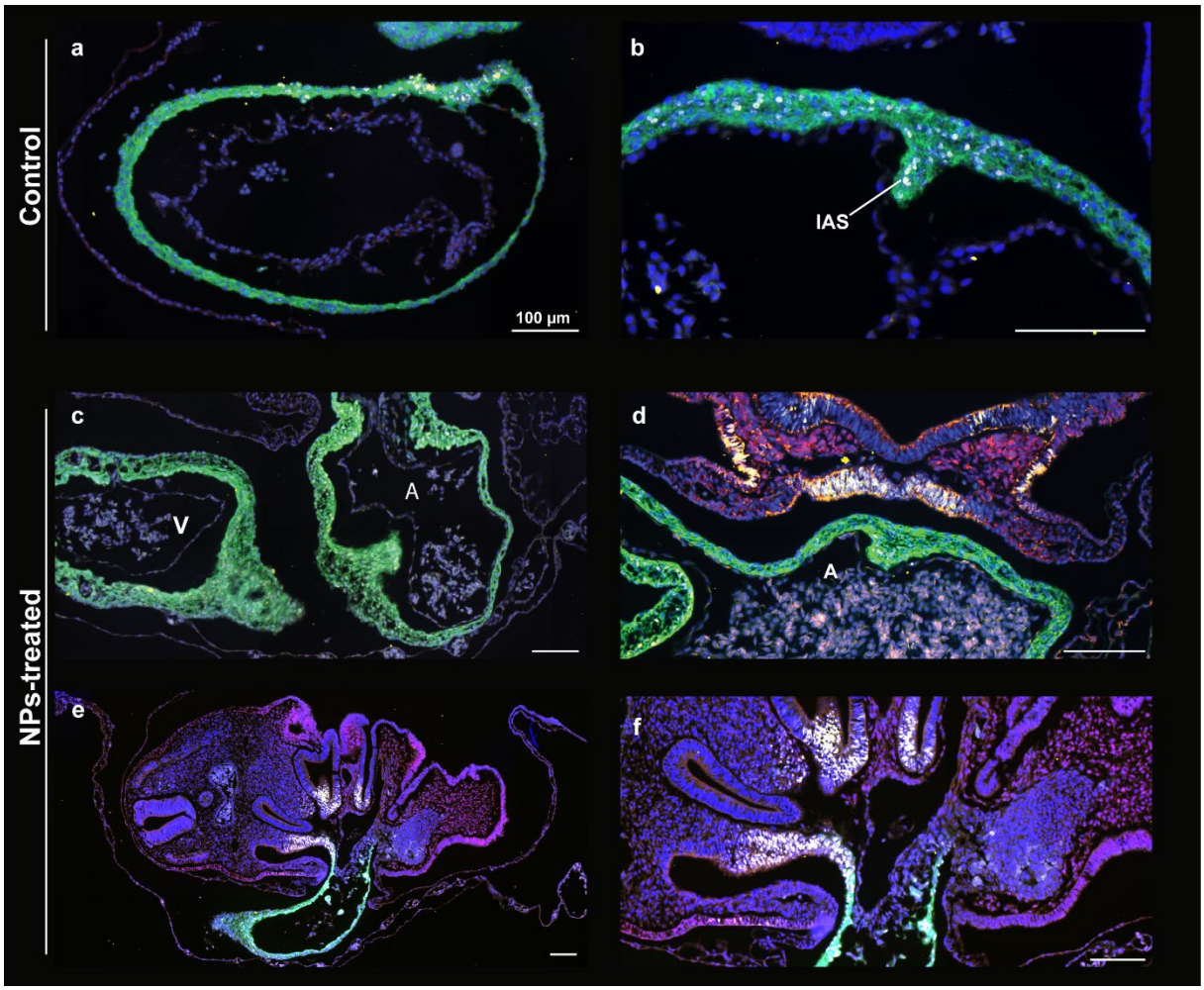

Fig. 3-7. **PS-NPs disrupt the development of the endocardial cushions of the heart in PS-NPs-treated chicken embryo at 2 dpe**. Immunochemistry for TFAP2A protein (AP-2α), NKX2-5 and cardiac TNNI performed on transverse sections of control and PS-NPs-treated chicken embryos at 2 dpe. **a** and **b**, control embryo, stage 18, *n* = 2, note the green staining TNNI in the cytoplasm and the NKX2-5 (yellow channel) in the nuclei of cells in the myocardium and inter-atrial septum. (**b**). **c**-**f**, PS-NPs-treated embryos, *n* = 5. **c**, stage 17. **d**, stage 20. **e** and **f**, both are stage 17. In **c** and **d**, the same staining has been observed in the myocardium of the PS-NPs-treated embryos. In **d**-**f**, note the NKX2-5 expression (yellow channel) in the endoderm and nuclei of the splanchnic mesoderm and myocardium. *Key*: A, atrium; IAS, inter-atrial septum; V, ventricle. Scale bars are all 100 µm. Blue, DAPI nuclear staining. Yellow, NKX2-5 protein staining. Red, TFAP2A protein staining. Green, TNNI protein staining.

The analysis of 3 dpe chick embryos

We found expression of NKX2-5 only in the PS-NPs-treated embryos, but less in control embryos (Fig. 3-8). It is highly likely that the weak staining was caused by technical problem, since that NKX2-5 play an essential role in the development of

cardiomyocytes and in cardiac precursors (Jamali et al., 2001; Paffett-Lugassy et al., 2013). We think the concentration of antibodies we used in the control embryos were relatively low. Among the PS-NP-treated embryos, the expression of NKX2-5 was located in the in the middle of the flow divider (Fig. 3-8e). In addition, the flow divider was unusually massive in some of the PS-NP-treated embryos (Fig. 3-8f). NKX2-5 expression was also observed at in the inflow end of the heart tube, continuing into the myocardium (Fig. 3-8g). Moreover, NKX2-5 staining was also observed in the ventricular wall (Fig. 3-8h). This expression was in the nuclei of the cells, most likely the excitatory cells of the heart muscle (Fig. 3-8h).

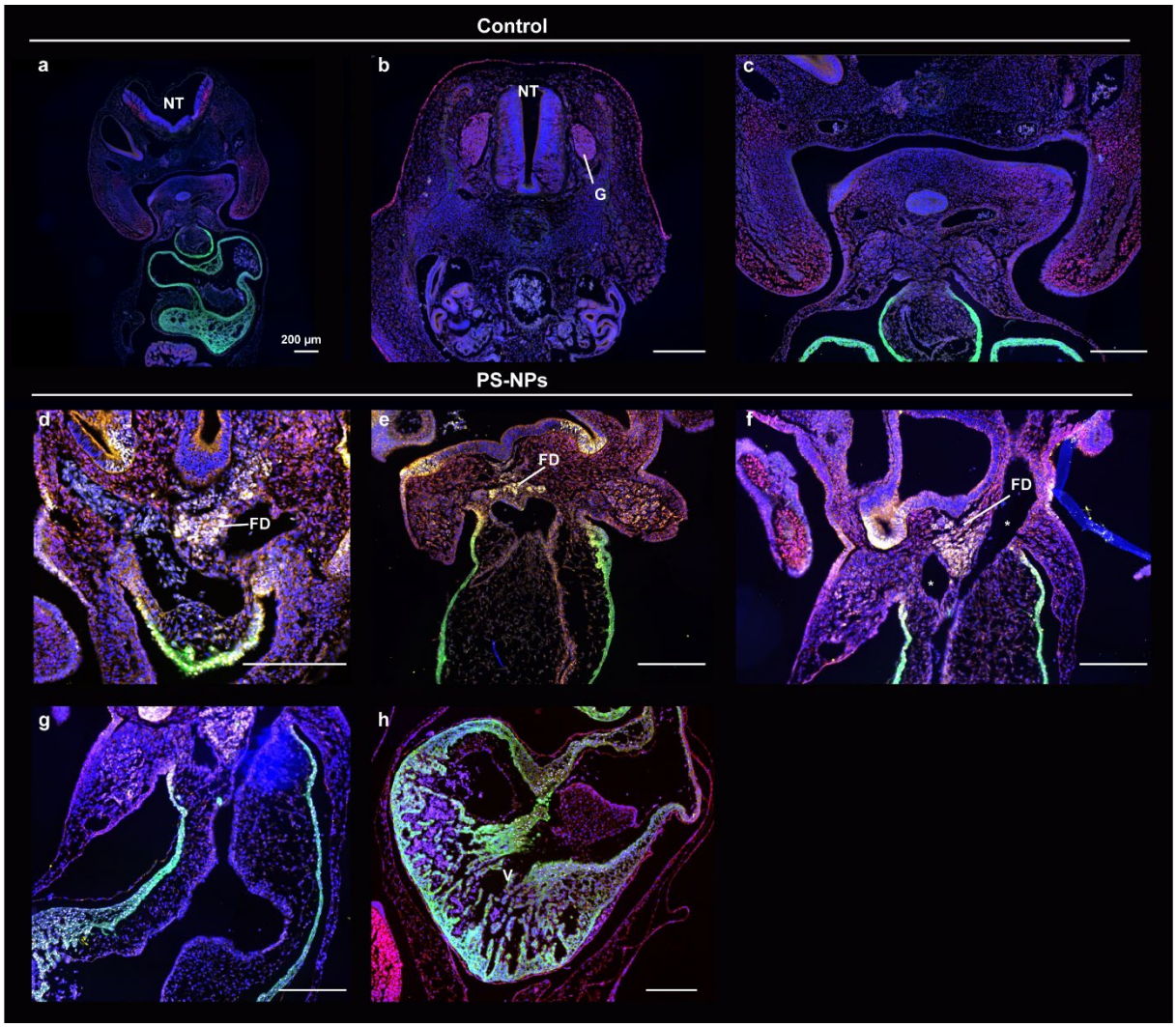

Fig. 3-8. **PS-NPs disrupt the development of the second heart field in the chicken embryos at 3 dpe**. **a**-**c**, control embryo, stage 23. **d**-**f**, PS-NPs-treated embryos. **d**, stage 24, **e**, stage 22, **f**-**h**, stage 21. Note the red staining in the ectoderm in (**a**), ganglia (**b**) and pharyngeal arches (**c**). Little or no NKX2-5 expression is seen in control embryos, but strong expression is seen in PS-NPs-treated embryos.

NKX2-5 expression (yellow channel) was observed in nuclei of the flow divider (**d**-**f**). Yellow staining was also observed at the start of the heart tube, continuing into the myocardium (**f**-**h**). Key: Asterisk (*), double outflow tract; FD, flow divider; G, ganglion; NT, neural tube; V, Ventricle. Blue, DAPI nuclear staining. Yellow, NKX2-5 protein staining. Red, TFAP2A protein staining. Green, TNNI protein staining.

Discussion

We have described a wide spectrum of severe malformations in chicken embryos exposed *in ovo* to 25 nm PS-NPs. The malformations include neural tube and craniofacial defects, as noted previously (Nie et al., 2021). In addition to those reported before, we found heart malformations, bradycardia, persistent or extra pharyngeal arch arteries, maxillary hypoplasia, axial defects, tail aplasia and, in one specimen, bilateral phocomelia of the hindlimbs. We also found that treated embryos showed defective cellularization of the cardiac jelly, thinned myocardium and reduced diameter of some blood vessels. This is a much wider spectrum of malformations than previously reported, and the congenital heart defects are reported here for the first time.

It has previously been shown that such malformations can also be produced in the chicken embryo by surgical ablation of the cardiac neural crest (Keyte and Hutson, 2012; Kirby and Waldo, 1995), that is, the crest cells at the axial level between the otocyst and somite three (Hutson and Kirby, 2007). The early-stage cardiovascular abnormalities, including altered hemodynamics that we observed have also been reported in other studies in which pre-migratory cardiac neural crest were surgically ablated (Kirby and Waldo, 1990; Waldo et al., 1999). At later stages, treated embryos showed instances of abnormal branching of the pharyngeal arch arteries, ventricular septal defects and aortopulmonary septal defects. These malformations likely arise because of damage to the neural crest, which is essential for normal development of the aortopulmonary septal complex of the heart and the wall of the great vessels (Erhardt et al., 2021; Hutson and Kirby, 2007; Kirby and Waldo, 1995; Newbern et al., 2008; Poelmann et al., 1998; Porras and Brown, 2008). We also observed epicardial

blebbing, probably caused by disturbed fluid handling of the developing coronary system that showed scant arterial development and no ingrowth into the neural crest-dependent aortic root (Gittenberger-de Groot et al., 2012). We also noted ectopia cordis, a phenotype associated with congenital cardiac malformations in human such as double outlet right ventricle (Malik et al., 2015).

In addition, we have observed thinner myocardium in the outflow tract compared to the ventricle in PS-NPs-treated embryo. This suggests that either the migration of the neural crest cells is arrested, or perhaps their signaling is affected. It could be that PS-NPs affect the development of the second heart field. The presence of neural crest cells is needed for normal second heart field development (Waldo et al., 2005). The second heart field is a population of cells located around the ventral caudal pharynx which plays an important role in lengthening of the outflow tract, and for the proper alignment of the aorta and pulmonary trunk with respect to the septal complex. Disruption of these processes can already be detected early, that is, before the neural crest cells reach the outflow tract (Keyte and Hutson, 2012). If cardiac neural crest cells are ablated experimentally, the myocardial cells from the second heart field may fail to be incorporated normally into the myocardium, causing abnormal looping of the heart (Yelbuz et al., 2002).

In addition to cardiac malformations, we often saw hypoplasia or aplasia of the upper beak, and failure of Meckel's cartilage to fuse with its contralateral partner. The co-occurrence of cardiac and craniofacial malformations in our study is consistent with the fact that the cranial neural crest contributes to the development of both the heart and the facial skeleton (Keyte and Hutson, 2012). The idea of a mechanistic link between cardiac and craniofacial development is embodied in the concept of the 'cardiocraniofacial module' (Keyte and Hutson, 2012). Furthermore an association of cardiac and craniofacial malformations is seen in clinical syndromes such as DiGeorge syndrome (chromosome 22q11.2 deletion syndrome) (McDonald-McGinn and Sullivan, 2011).

Our results show that 25 nm PS-NPs cause various cardiac and vascular defects in the chicken embryo. These defects include: excess cardiac jelly with a lack of epithelial mesenchymal transition, thin epicardium and myocardium, ventricular septal defect, persistent truncus arteriosus and supernumerary arteries. One of these defects alone, or a combination of defects, probably explain the abnormal cardiac function that we observed (lower heart rate and abnormal blood flow) in PS-NPs-treated embryos. We speculate that these cardiac effects could result in high mortality rate among PS-NPs-treated embryos. In Chapter 4, we will explore the potential cellular mechanisms of PS-NP toxicity to embryos.

References

Abd-Elgaliel, W. R. and Tung, C. H. (2012). A Cardiac Tissue-Specific Binding Agent of Troponin I. *Mol Biosyst* **8**, 2629-2632.

Anagnosti, L., Varvaresou, A., Pavlou, P., Protopapa, E. and Carayanni, V. (2021). Worldwide Actions against Plastic Pollution from Microbeads and Microplastics in Cosmetics Focusing on European Policies. Has the Issue Been Handled Effectively? *Marine Pollution Bulletin* **162**, 111883.

Bamforth, S. D., Braganca, J., Eloranta, J. J., Murdoch, J. N., Marques, F. I., Kranc, K. R., Farza, H., Henderson, D. J., Hurst, H. C. and Bhattacharya, S. (2001). Cardiac Malformations, Adrenal Agenesis, Neural Crest Defects and Exencephaly in Mice Lacking Cited2, a New Tfap2 Co-Activator. *Nat Genet* **29**, 469-474.

Bancroft, J. D. and Gamble, M. (2008). *Theory and Practice of Histological Techniques*: Elsevier Health Sciences.

Boehnke, N., Straehla, J. P., Safford, H. C., Kocak, M., Rees, M. G., Ronan, M., Rosenberg, D., Adelmann, C. H., Chivukula, R. R., Nabar, N., et al. (2022). Massively Parallel Pooled Screening Reveals Genomic Determinants of Nanoparticle Delivery. *Science* **377**, eabm5551.

Brewer, S., Jiang, X., Donaldson, S., Williams, T. and Sucov, H. M. (2002). Requirement for Ap-2alpha in Cardiac Outflow Tract Morphogenesis. *Mech Dev* **110**, 139-149.

Cotti, S., Huysseune, A., Koppe, W., Rücklin, M., Marone, F., Wölfel, E. M., Fiedler, I. A., Busse, B., Forlino, A. and Witten, P. E. (2020). More Bone with Less Minerals? The Effects of Dietary Phosphorus on the Post-Cranial Skeleton in Zebrafish. *International Journal of Molecular Sciences* **21**, 5429.

Cox, K. D., Covernton, G. A., Davies, H. L., Dower, J. F., Juanes, F. and Dudas, S. E. (2019). Human Consumption of Microplastics. *Environmental Science & Technology* **53**, 7068-7074.

de Bakker, M. A. G., Fowler, D. A., Oude, K. d., Dondorp, E. M., Navas, M. C. G., Horbanczuk, J. O., Sire, J.-Y., Szczerbińska, D. and Richardson, M. K. (2013). Digit Loss in Archosaur Evolution and the Interplay between Selection and Constraints. *Nature* **500**, 445-448.

Erhardt, S., Zheng, M., Zhao, X., Le, T. P., Findley, T. O. and Wang, J. (2021). The Cardiac Neural Crest Cells in Heart Development and Congenital Heart Defects. *J Cardiovasc Dev Dis* **8**.

European_Commission (2022). Commission Regulation (Eu) Amending Annex Xvii to Regulation (Ec) No 1907/2006 of the European Parliament and of the Council Concerning the Registration, Evaluation, Authorisation and Restriction of Chemicals (Reach) as Regards Synthetic Polymer Microparticles. pp. 12. Brussels.

Feng, M., Luo, J., Wan, Y., Zhang, J., Lu, C., Wang, M., Dai, L., Cao, X., Yang, X. and Wang, Y. (2022). Polystyrene Nanoplastic Exposure Induces Developmental Toxicity by Activating the Oxidative Stress Response and Base Excision Repair Pathway in Zebrafish (Danio Rerio). *ACS omega* **7**, 32153-32163.

Gittenberger-de Groot, A. C., Winter, E. M., Bartelings, M. M., Goumans, M. J., DeRuiter, M. C. and Poelmann, R. E. (2012). The Arterial and Cardiac Epicardium in Development, Disease and Repair. *Differentiation* **84**, 41-53.

Hutson, M. R. and Kirby, M. L. (2007). Model Systems for the Study of Heart Development and Disease. Cardiac Neural Crest and Conotruncal Malformations. *Semin Cell Dev Biol* **18**, 101-110.

Jamali, M., Rogerson, P. J., Wilton, S. and Skerjanc, I. S. (2001). Nkx2–5 Activity Is Essential for Cardiomyogenesis*. *Journal of Biological Chemistry* **276**, 42252-42258.

Jenner, L. C., Rotchell, J. M., Bennett, R. T., Cowen, M., Tentzeris, V. and Sadofsky, L. R. (2022). Detection of Microplastics in Human Lung Tissue Using Mftir Spectroscopy. *Sci Total Environ* **831**, 154907.

Keyte, A. and Hutson, M. R. (2012). The Neural Crest in Cardiac Congenital Anomalies. *Differentiation* **84**, 25-40.

Kirby, M. L. and Waldo, K. L. (1990). Role of Neural Crest in Congenital Heart Disease. *Circulation* **82**, 332-340.

Kirby, M. L. and Waldo, K. L. (1995). Neural Crest and Cardiovascular Patterning. *Circ.Res.* **77**, 211-215.

Koelmans, A. A., Nor, N. H. M., Hermsen, E., Kooi, M., Mintenig, S. M. and De France, J. (2019). Microplastics in Freshwaters and Drinking Water: Critical Review and Assessment of Data Quality. *Water research*.

Kögel, T., Bjorøy, Ø., Toto, B., Bienfait, A. M. and Sanden, M. (2020). Micro-and Nanoplastic Toxicity on Aquatic Life: Determining Factors. *Science of The Total Environment* **709**, 136050-136050.

Leslie, H. A., van Velzen, M. J. M., Brandsma, S. H., Vethaak, A. D., Garcia-Vallejo, J. J. and Lamoree, M. H. (2022). Discovery and Quantification of Plastic Particle Pollution in Human Blood. *Environ Int* **163**, 107199.

Mai, C. T., Isenburg, J. L., Canfield, M. A., Meyer, R. E., Correa, A., Alverson, C. J., Lupo, P. J., Riehle-Colarusso, T., Cho, S. J., Aggarwal, D., et al. (2019). National Population-Based Estimates for Major Birth Defects, 2010–2014. *Birth Defects Research* **111**, 1420-1435.

Malik, R., Zilberman, M. V., Tang, L., Miller, S. and Pandian, N. G. (2015). Ectopia Cordis with a Double Outlet Right Ventricle, Large Ventricular Septal Defect, Malposed Great Arteries and Left Ventricular Hypoplasia. *Echocardiography* **32**, 589-591.

Marone, F., Studer, A., Billich, H., Sala, L. and Stampanoni, M. (2017). Towards on-the-Fly Data Post-Processing for Real-Time Tomographic Imaging at Tomcat. *Advanced Structural and Chemical Imaging* **3**, 1-11.

McClelland, K. S., Ng, E. T. and Bowles, J. (2016). Agarose/Gelatin Immobilisation of Tissues or Embryo Segments for Orientated Paraffin Embedding and Sectioning. *Differentiation* **91**, 68-71.

McCulley, D. J. and Black, B. L. (2012). Chapter Nine - Transcription Factor Pathways and Congenital Heart Disease. In *Current Topics in Developmental Biology* (ed. B. G. Bruneau), pp. 253-277: Academic Press.

McDonald-McGinn, D. M. and Sullivan, K. E. (2011). Chromosome 22q11.2 Deletion Syndrome (Digeorge Syndrome/Velocardiofacial Syndrome). *Medicine (Baltimore)* **90**, 1-18.

Mitrano, D. M., Wick, P. and Nowack, B. (2021). Placing Nanoplastics in the Context of Global Plastic Pollution. *Nature Nanotechnology* **16**, 491-500.

Newbern, J., Zhong, J., Wickramasinghe, R. S., Li, X., Wu, Y., Samuels, I., Cherosky, N., Karlo, J. C., O'Loughlin, B., Wikenheiser, J., et al. (2008). Mouse and Human Phenotypes Indicate a Critical Conserved Role for Erk2 Signaling in Neural Crest Development. *Proc Natl Acad Sci U S A* **105**, 17115-17120.

Nie, J.-h., Shen, Y., Roshdy, M., Cheng, X., Wang, G. and Yang, X. (2021). Polystyrene Nanoplastics Exposure Caused Defective Neural Tube Morphogenesis through Caveolae-Mediated Endocytosis and Faulty Apoptosis. *Nanotoxicology*, 1-20.

Paffett-Lugassy, N., Singh, R., Nevis, K. R., Guner-Ataman, B., O'Loughlin, E., Jahangiri, L., Harvey, R. P., Burns, C. G. and Burns, C. E. (2013). Heart Field Origin of Great Vessel Precursors Relies on Nkx2.5-Mediated Vasculogenesis. *Nature Cell Biology* **15**, 1362-1369.

Paganin, D., Mayo, S. C., Gureyev, T. E., Miller, P. R. and Wilkins, S. W. (2002). Simultaneous Phase and Amplitude Extraction from a Single Defocused Image of a Homogeneous Object. *Journal of Microscopy* **206**, 33-40.

Pitt, J. A., Kozal, J. S., Jayasundara, N., Massarsky, A., Trevisan, R., Geitner, N., Wiesner, M., Levin, E. D. and Di Giulio, R. T. (2018). Uptake, Tissue Distribution, and Toxicity of Polystyrene Nanoparticles in Developing Zebrafish (*Danio Rerio*). *Aquatic Toxicology* **194**, 185-194.

Poelmann, R. E., Mikawa, T. and Gittenberger-de Groot, A. C. (1998). Neural Crest Cells in Outflow Tract Septation of the Embryonic Chicken Heart: Differentiation and Apoptosis. *Dev Dyn* **212**, 373-384.

Porras, D. and Brown, C. B. (2008). Temporal-Spatial Ablation of Neural Crest in the Mouse Results in Cardiovascular Defects. *Dev Dyn* **237**, 153-162.

Schwabl, P., Köppel, S., Königshofer, P., Bucsics, T., Trauner, M., Reiberger, T. and Liebmann, B. (2019). Detection of Various Microplastics in Human Stool: A Prospective Case Series. *Ann Intern Med* **171**, 453-457.

Stampanoni, M., Groso, A., Isenegger, A., Mikuljan, G., Chen, Q., Bertrand, A., Henein, S., Betemps, R., Frommherz, U. and Böhler, P. (2006). Trends in Synchrotron-Based Tomographic Imaging: The Sls Experience. In *Developments in X-ray Tomography V*, pp. 193-206: SPIE.

Sulukan, E., Şenol, O., Baran, A., Kankaynar, M., Yıldırım, S., Kızıltan, T., Bolat, İ. and Ceyhun, S. B. (2022). Nano-Sized Polystyrene Plastic Particles Affect Many Cancer-Related Biological Processes Even in the Next Generations; Zebrafish Modeling. *Science of The Total Environment* **838**, 156391.

Vighi, M., Bayo, J., Fernández-Piñas, F., Gago, J., Gómez, M., Hernández-Borges, J., Herrera, A., Landaburu, J., Muniategui-Lorenzo, S. and Muñoz, A.-R. (2021). Micro and Nano-Plastics in the Environment: Research Priorities for the near Future. *Reviews of Environmental Contamination and Toxicology Volume 257*, 163-218.

Waldo, K., Zdanowicz, M., Burch, J., Kumiski, D. H., Stadt, H. A., Godt, R. E., Creazzo, T. L. and Kirby, M. L. (1999). A Novel Role for Cardiac Neural Crest in Heart Development. *J Clin Invest* **103**, 1499-1507.

Waldo, K. L., Hutson, M. R., Stadt, H. A., Zdanowicz, M., Zdanowicz, J. and Kirby, M. L. (2005). Cardiac Neural Crest Is Necessary for Normal Addition of the Myocardium to the Arterial Pole from the Secondary Heart Field. *Dev Biol* **281**, 66-77.

Wan, J.-K., Chu, W.-L., Kok, Y.-Y. and Lee, C.-S. (2018). Distribution of Microplastics and Nanoplastics in Aquatic Ecosystems and Their Impacts on Aquatic Organisms, with Emphasis on Microalgae. *Reviews of Environmental Contamination and Toxicology Volume 246*, 133-158.

Xu, Q. and Wilkinson, D. G. (1998). In Situ Hybridization of Mrna with Hapten Labelled Probes. *In Situ Hybridisation: A Practical Approach*, 87-106.

Yelbuz, T. M., Waldo, K. L., Kumiski, D. H., Stadt, H. A., Wolfe, R. R., Leatherbury, L. and Kirby, M. L. (2002). Shortened Outflow Tract Leads to Altered Cardiac Looping after Neural Crest Ablation. *Circulation* **106**, 504-510.

Zhang, J., Wang, L. and Kannan, K. (2020). Microplastics in House Dust from 12 Countries and Associated Human Exposure. *Environment international* **134**, 105314.

Zhang, Y., Yin, K., Wang, D., Wang, Y., Lu, H., Zhao, H. and Xing, M. (2022). Polystyrene Microplastics-Induced Cardiotoxicity in Chickens Via the Ros-Driven Nf-Kb-Nlrp3-Gsdmd and Ampk-Pgc-1α Axes. *Science of The Total Environment* **840**, 156727.

Zhu, X., Wang, C., Duan, X., Liang, B., Genbo Xu, E. and Huang, Z. (2023). Micro- and Nanoplastics: A New Cardiovascular Risk Factor? *Environment International* **171**, 107662.